HHS Public Access

Author manuscript

Cells Tissues Organs. Author manuscript; available in PMC 2019 October 09.

Published in final edited form as:

Cells Tissues Organs. 2018 ; 205(5-6): 279–292. doi:10.1159/000492973.

Na^+/H^+ exchangers are required for development and function of vertebrate mucociliary epithelia

Dingyuan I. Sun[1,2], **Alexia Tasca**[3], **Maximilian Haas**[3], **Grober Baltazar**[1,4], **Richard M. Harland**[1], **Walter E. Finkbeiner**[2], and **Peter Walentek**[1,3,*]

[1]Molecular and Cell Biology Department, Genetics, Genomics and Development Division, University of California, Berkeley, CA, USA

[2]Department of Pathology, University of California, San Francisco, CA, USA

[3]Renal Division, Department of Medicine, University Freiburg Medical Center, Freiburg, Germany

[4]Current address: Children's Medical Research Institute, Westmead, Australia

Abstract

Na^+/H^+exchangers (NHEs) represent a highly conserved family of ion transporters that regulate pH homeostasis. NHEs as well as other proton transporters were previously linked to regulation of the Wnt signaling pathway, cell polarity signaling and mucociliary function. Furthermore, mutations in the gene *SLC9A3* (encoding NHE3) were detected as additional risk factors for airway infections in cystic fibrosis patients. Here, we used the *Xenopus* embryonic mucociliary epidermis as well as human airway epithelial cells (HAECs) as models to investigate the functional roles of NHEs in mucociliary development and regeneration. In *Xenopus* embryos, NHEs 1-3 were expressed during epidermal development, and loss of NHE function impaired mucociliary clearance in tadpoles. Clearance defects were caused by reduced cilia formation and disrupted alignment of basal bodies in multiciliated cells as well as dysregulated mucociliary gene expression. These data also suggested that NHEs may contribute to the activation of Wnt signaling in mucociliary epithelia. In HAECs, pharmacological inhibition of NHE function also caused defective ciliation and regeneration in airway multiciliated cells. Collectively, our data revealed a requirement for NHEs in vertebrate mucociliary epithelia and linked NHE activity to cilia formation and function in differentiating multiciliated cells. Our results provide an entry point for the understanding of NHE contribution to signaling, development, and pathogenesis of the human respiratory tract.

Keywords

Slc9a1; Slc9a2; Slc9a3; NHE1; NHE2 NHE3; cilia; airway; Xenopus

*Correspondence should be sent to: Dr. Peter Walentek, University Clinic Freiburg, Department of Internal Medicine IV (Nephrology and General Medicine) and ZBSA – Center for Biological Systems Analysis, Habsburgerstr. 49, 79104 Freiburg, Germany, Telephone: +49-761-203-97206, peter.walentek@medizin.uni-freiburg.de.

Authors contributions:

DIS contributed to experimental design, data analysis and manuscript preparation, performed most experiments including Xenopus manipulations, ALI cultures, IF, ISH and imaging. AT, MH and GB contributed to molecular cloning and ISH. WEF and RMH contributed to experimental design and interpretation of data. PW determined the scope of the study, contributed to experimental design, experiments, data analysis and interpretation, and wrote the manuscript with input from all authors.

Introduction:

The family of transmembrane Na^+/H^+ exchangers (NHEs) is encoded by solute carrier genes *SLC9s*, which are subdivided into three groups *SLC9A-C* [Fuster, and Alexander, 2014], NHEs contribute to pH regulation of the cytoplasm and organelle content, and act in concert with other ion transporters to maintain cellular homeostasis by extruding protons in exchange for sodium ions [Slepkov et al., 2007; Souza et al., 1998; Schreiber, 2005], NHE1-5 (*SLC9A1-5*) predominantly localize to the cell membrane, while NHA1-2 (Na^+/H^+ antiporters, *SLC9B1-2*) localize mostly to intracellular sites, and *SLC9C1-2* genes encode one sperm-specific and one putative NHE form, respectively [Fuster, and Alexander, 2014], Additionally, multiple NHEs were shown to influence cell signaling and specific cell behavior *in vitro* and *in vivo*, including Wnt/planar cell polarity signaling, directional cell migration and embryonic development [Siyanov, and Baltz, 2013; Schneider et al., 2009; Ozkucur et al., 2014; Slepkov et al., 2007; Simons et al., 2009], Consequently, NHE function or dysregulation were implicated in human diseases, such as tumor formation and metastasis, and a higher susceptibility to airway infections in cystic fibrosis patients [Sera et al., 2012; Harguindey et al., 2005; Slepkov et al., 2007; Pereira et al., 2017a; Dorfman et al., 2011; Corvol et al., 2015; Li et al., 2014].

We have previously found that the gastric H^+/K^+ATPase (*atp4a*), which is also a transmembrane proton transporter, is required for efficient activation of the canonical Wnt/β-catenin as well as the non-canonical Wnt/planar cell polarity (PCP) signaling pathways during *Xenopus* embryonic development [Walentek et al., 2012], Loss of gastric H^+/K^+ATPase function or dysregulation of Wnt signaling impairs the formation and function of motile cilia in *Xenopus* embryos leading to defects of the left-right body axis and inner organ asymmetry, kidney failure and formation of fluid filled cysts, as well as hydrocephalus [Walentek et al., 2012; Walentek et al., 2015b], Additionally, we found that knockdown or pharmacological inhibition of the gastric H^+/K^+ATPase interferes with normal development and function of the embryonic mucociliary epidermis in *Xenopus* [Walentek et al., 2015a], The mucociliary epidermis of *Xenopus* embryos is composed of goblet and small secretory cells (SSCs) releasing mucus, antimicrobial peptides and other bioactive compounds, ion secreting cells (ISCs) regulating homeostasis, and multiciliated cells (MCCs) [Walentek, and Quigley, 2017], MCCs produce hundreds of motile cilia projecting from the apical surface to generate a directional extracellular fluid flow through coordinated beating of cilia [Brooks, and Wallingford, 2014], Canonical Wnt/β-catenin signaling regulates expression of the transcription factor *foxj1*, which activates downstream ciliary genes required for cilia assembly and motility and is therefore necessary for motile ciliogenesis [Walentek et al., 2012; Caron et al., 2012; Stubbs et al., 2008], In contrast, the non-canonical Wnt/PCP pathway regulates actin organization and provides polarity cues to align cilia for directional beating, a prerequisite for the generation of efficient extracellular fluid flow [Vladar et al., 2009; Wallingford, 2010], Over recent years, the *Xenopus* embryonic epidermis emerged as valuable model to study the biology and pathophysiology of airway mucociliary epithelia, whose function accounts for clearance of the mammalian respiratory tract [Walentek, and Quigley, 2017; Walentek et al., 2017], Impaired ciliogenesis and changes in cell type composition or differentiation lead to breakdown of mucociliary clearance and increase the

susceptibility to airway infections. Both conditions are frequently observed in ciliopathy patients or patients suffering from chronic obstructive pulmonary diseases, but in many instances the underlying molecular mechanisms remain unresolved.

Since NHEs were previously implicated in Wnt signaling regulation as well as airway diseases, we used *Xenopus* to investigate a potential role of NHE1-3 family members on the development and function of the mucociliary epidermis and ciliogenesis. Here, we provide data indicating that NHEs are required for normal mucociliary development, MCC ciliogenesis and cilia polarity in *Xenopus* embryos as well as normal MCC ciliation during regeneration of human airway epithelial cells *in vitro.* Thus, our data provide an entry point to elucidate the influence of proton transporters on cilia formation in mucociliary epithelia and on human health.

Materials and Methods:

Manipulation of *Xenopus* Embryos, Constructs and In Situ Hybridization

X. laevis eggs were collected and *in vitro*-fertilized, then cultured and microinjected by standard procedures [Sive et al., 2000], Embryos were injected with Morpholino oligonucleotides (MOs, Gene Tools) and mRNAs at the four-cell stage using a PicoSpritzer setup in 1/3× Modified Frog Ringer's solution (MR) with 2.5% Ficoll PM 400 (GE Healthcare, #17-0300-50), and were transferred after injection into 1/3× MR containing Gentamycin. Drop size was calibrated to about 7–8 nL per injection. Rhodamine-B dextran (0.5–1.0 mg/mL; Invitrogen, #D1841) or indicated mRNAs were co-injected and used as lineage tracers.

Morpholino oligonucleotides were obtained from Gene Tools.

slc9a1 MO (5'-AGTTTAGAAGCACTTTCTTCCCCAT-3') targeting NCBI entry NM_001088084.1, *slc9a2* MO (5'-GCTGATGTACCACCGGAAAGCCCAT-3') targeting NCBI entry XM_018247081.1, *slc9a3* MO (5'-CAGCATGGAGTTGAGGCCACTTCTC-3') targeting NCBI entry XM_018267666.1, were administered at doses ranging between 11.3ng (1.33pmol), to 34 and 51ng (or 4-6pmol). A morpholino oligonucleotide targeting *Xenopus hvcn1* was used for control injections at 4-6pmol (*hvcn1* MO 5'-TGGCGCAGGCACCCAGCCATTTTAC-3'). mRNAs encoding Centrin4-CFP [Antoniades et al., 2014; Park et al., 2008], Clamp-RFP [Mitchell et al., 2009] were prepared using the Ambion mMessage Machine kit using Sp6 (#AM1340) and diluted to 50 ng/μL (400pg per injection) for injection into embryos.

Drug treatment of embryos started at stage 8 and embryos were fixed at stage 29. 200μM 5-(N-ethyl-N-isopropyl)-Amiloride (ElPA; Sigma, #A3085) suspended in DMSO (Sigma, #D2650) was added to the medium. An equal amount of DMSO without EIPA was used as vehicle control.

Xenopus laevis slc9a cDNA for anti-sense *in situ* hybridization probes was derived from total RNA extracts and cloned using the following primers (shown 5' to 3') and standard RT-PCR:

slc9a1-f TCCCAAGAGAAATGTTCCTAACTG

slc9a1-r ACTCAGGCATCGTTGAAGAC

(matching NCBI entry NM_001088084.1)

slc9a2-f CCCATCTTTGTCTTCATTATCCAC

slc9a2-r TCTTGGTATTTGTGCTTTGTCCTG

(matching NCBI entry XM_018247081.1)

slc9a3-f TCTGCCATTGAAGATGTTTCTG

slc9a3-r GGGTAGCATAGTCATTGTACTG

(matching NCBI entry XM_018267666.1)

DNAs were purified using the PureYield Midiprep kit (Promega, #A2495) and were linearized before in vitro synthesis of anti-sense RNA probes using T7 polymerase (Promega, #P2077) and Dig-labeled rNTPs (Roche, #3359247910 and 11277057001). Embryos were *in situ* hybridized according to [Harland, 1991], bleached after staining and imaged using a Zeiss AxioZoom setup. Section were made after embedding in gelatin-albumin with glutaraldehyde and sectioned at 50μm as described in [Walentek et al., 2012].

Air-liquid interface (ALI) culture of Human Airway Epithelial cells (HAECs) and EIPA treatment

Bronchial tissues were obtained from subjects after lung transplantation or from lungs donated for transplant but subsequently found to be unsuitable for that purpose. Human bronchial epithelial (HBE) cells were isolated after incubation in 1 mg/ml Protease (Sigma, #P5147) solution overnight at 4 °C. HBE cells from 3 donors were plated at 166,666 cells per 12 mm transwell insert (Corning, Costar #3460) precoated with 15 μg/cm^2 human placental collagen (Sigma, #C7521). Cultures were grown at an air-liquid interface (ALI) in 1 ml-1.5 ml ALI medium per well at 37°C in 5% CO_2/95% air, as previously described [Namkung et al., 2010].

Medium was changed every 2-3 days. 25μM 5-(N-ethyl-N-isopropyl)-Amiloride (EIPA; Sigma, #A3085) suspended in DMSO (Sigma, #D2650) was added to the medium for 7 days starting on ALI day 1, 8, 15 or day 22. After treatment, cultures were further cultivated to ALI day 28, then rinsed with PBS (Mediatech, #21-030-CV) and fixed for 2 h in 4% Paraformaldehyde. Transwell inserts were then cut away from the plastic supports, divided in halves and processed for immunohistochemical or routine histological studies as described below.

Statistical Evaluation

Statistical evaluation of experimental data was performed using chi-squared tests (http://www.physics.csbsju.edu/stats/contingency.html) for all data depicted by stacked bar-graphs,

or Wilcoxon sum of ranks (Mann-Whitney) tests (http://astatsa.com/WilcoxonTest/) for all data depicted by box-plots.

Immunofluorescence Staining and Sample Preparation

For *Xenopus* immunofluorescence, whole embryos were fixed at embryonic stages 30-33 (mucociliary MCCs) in 4% paraformaldehyde at 4°C over-night. Embryos were washed 3× 15 min with PBS, 2× 30 min in PBST (0.1% Triton X-100 in PBS), and were blocked in PBST-CAS (90% PBS containing 0.1% Triton X-100, 10% CAS Blocking; ThermoFischer #00-8120) for 1h at RT. Primary and secondary antibodies were applied in 100% CAS Blocking over night at 4°C. Actin was stained by incubation (30-60 min at room temperature) with AlexaFluor 488-labeled Phalloidin (1:40 in PBSt; Molecular Probes #A12379), mucus-like compounds were stained by incubation (over night at 4°C) with AlexaFluor 647-labeled PNA (1:1000 in PBSt; Molecular Probes #L32460).

For whole mount immunofluorescence staining of human airway epithelial cells (HAECs), fixed cultures were processed for staining as described for *Xenopus* samples. For sections of HAECs, fixed HAECs on cell culture inserts were processed in an automated tissue processor (Tissue-Tek VIP, Sakura Finetek, USA, Torrence, CA) and embedded on edge in paraffin. Paraffin microscopic section (5μm) were de-waxed in xylene and rehydrated through a graduated alcohol series and water. Sections were either stained with hematoxylin and eosin (H&E) or proceeded for immunofluorescence staining as described for Xenopus samples after submerging the sections in reveal decloaker solution (Biocare Medical #RV1000M) and heating for 10 minutes at 125°C for antigen retrieval.

Primary antibodies: mouse monoclonal anti-Acetylated-α-tubulin (1:700; Sigma #T6793), rabbit polyclonal anti-Cytokeratin 5 antibody (1:100; Invitrogen #PA1-37974). Secondary antibodies (1:250): AlexaFluor 555-labeled goat anti-mouse antibody (Molecular Probes #A21422), AlexaFlour 488-labeled goat anti-rabbit antibody (Molecular Probes #R37116). Z-stack analysis and processing were done using ImageJ. Confocal imaging was conducted using a Zeiss LSM700 or Zeiss LSM880. Whole mount embryos were imaged on a Zeiss AxioZoom setup. DAPI was used to label nuclei (applied for 30 min. at room temperature, 1:100 in PBSt; Molecular Probes #D1306).

Imaging of Extracellular Fluid Flow

For imaging of extracellular fluid flow, control and manipulated stage 32 embryos were anesthetized (Benzocaine, Sigma #E1501) and exposed to latex beads (FluoSpheres® carboxylate-modified microspheres, 0.5 μm, red fluorescence [580/605], 2% solids, Invitrogen #F-8812; diluted to 0.04% in 1/3 × MR) in a sealed flow chamber. Time-lapse movies (10 sec / 50-100 frames per sec) were recorded using epifluorescence illumination at 20× magnification on a Zeiss Axioskop 2 in combination with a high-speed GX-1Memrecam (NACImage Technology) and processed in ImageJ for brightness/contrast. Particle linking, tracking and quantification of extracellular fluid flow velocities was performed as previously described using the Particle Tracker plugin for ImageJ and a customized R-script [Walentek et al., 2016; Walentek et al., 2015a], Flow movie depicts a

1:2 frame-reduced and size-reduced version of the original file to reduce file size. The movie plays at real time speed (25fps).

Sample size and analysis

Sample sizes for all experiments were chosen based on previous experience and used embryos derived from at least two different females. No randomization or blinding was applied.

Ethics statements on animal experiments and human research

This work was done with approval of University of California, Berkeley's Animal Care and Use Committee. University of California, Berkeley's assurance number is A3084-01, and is on file at the National Institutes of Health Office of Laboratory Animal Welfare. Human tissues were collected and used with approval from the University of California, San Francisco Committee on Human Research.

Results:

To investigate the potential roles of NHEs in the mucociliary embryonic epidermis, we first analyzed the expression of *slc9a1, 2* and *3* during early *Xenopus* development. To generate anti-sense RNA-probes for *slc9a1, 2* and 3, we cloned a C-terminal portion from each transcript, the portion where coding sequences are most divergent between the closely related gene family members (not shown). Our analysis revealed dynamic expression of all *slc9a* genes, including in epidermal precursors or the embryonic epidermis (Fig. 1). *slc9a1* and *3* were maternally deposited, while *slc9a2* was only expressed in later stages (Fig. 1 and S1B). Importantly, *slc9a1* was most strongly expressed, while *slc9a2* and *slc9a3* showed lower, but significant expression levels, which were confirmed by semi-quantitative reverse-transcription PCR on cDNAs derived from stages 2 - 31 (Fig. S1B) and analysis of independently generated RNA-sequencing data on mucociliary organoids during epidermal development (published elsewhere). *slc9a* genes were also expressed in the presomitic mesoderm or somites, the otic vesicle, cement gland, pronephros and the stomach/small intestine revealing overlapping but not identical expression patterns (Fig. 1 and S1A). Taken together, these data supported a possible functional role for NHEs during development and/or function of the mucociliary embryonic epidermis. Furthermore, in all cases epidermal expression domains were homogeneous and not in a dotted pattern, indicating a broad function throughout the epidermis, rather than functional restriction to one particular epidermal cell type.

Next, we designed morpholino oligonucleotides (MOs) specifically targeting the translational start site (ATG) of *slc9a1-3* transcripts and conducted MO-mediated knockdown experiments. We injected MOs unilaterally into both right blastomeres at the four-cell stage (st. 3) leaving the left two blastomeres unmanipulated. Thus, the left side of the embryo could be used as an internal control (Fig. S1C). Injection of *slc9a1*MO, *slc9a2*MO or *slc9a3*MO each resulted in similar phenotypes during tadpole stages (st. 45), leading to malformations of head structures, reduced eye size and impaired gut morphogenesis (Fig. S1C). Additionally, loss of NHE3 function (*slc9a3*MO) also caused

cyst formation and bloating of tadpoles (Fig. S1C), indicating kidney malfunction. Notably, higher concentrations of *slc9a2*MO (6pmol) had to be used and generated a relatively mild phenotype as compared to *slc9a1*MO and *slc9a3*MO (4pmol). Furthermore, combined knockdown of *slc9a1, 2* and *3* using 1.33pmol of each individual MO (4pmol total) generated a more drastic phenotype at stage 40 than single injection of *slc9a1, 2* or *3* MO at 4pmol, suggesting cooperative function of those NHEs at the cellular level during development (Fig. S1D). These data supported the conclusion that knockdown of *slc9a1-3* transcripts occurred upon MO injection and revealed similar developmental phenotypes as previously reported for gastric H^+/K^+ATPase loss-of-function, disruption of ciliary genes or knockdown of Wnt signaling components.

To test the effects of NHE1, 2 and 3 loss-of-function on mucociliary cells, we first analyzed the generation of extracellular fluid flow along the mucociliary epidermis in control and MO-injected embryos. For that, we knocked down *slc9a1, slc9a2 or slc9a3* individually and analyzed flow generation by application of fluorescent beads to the medium, epifluorescence imaging and particle tracking. Knockdown of either *slc9a1, slc9a2* or *slc9a3* resulted in a significant reduction in fluid flow velocity (Fig. 2A, Supplemental Movie 1), revealing defective mucociliary function in morphant embryos. Next, we injected MOs as described above, but in combination with mRNAs encoding basal body (Centring and rootlet (Clamp) proteins fused to CFP and RFP, respectively. Control and manipulated embryos were then analyzed by immunofluorescence and confocal microscopy to investigate cilia formation. In contrast to control-injected specimens, which displayed fully ciliated multiciliated cells (MCCs), MO-injected embryos formed MCCs with fewer and shorter cilia projecting from their apical surface (Fig. 2B, B'-B""). Importantly, MCC cilia defects appeared to be cell-autonomous, because non-targeted MCCs remained fully ciliated (non-CFP/RFP positive MCCs, indicated by asterisks in Fig. 2B). While most targeted MCCs in *slc9a1* morphants showed a strong reduction in ciliation, the effects of *slc9a2*MO and *slc9a3*MO were less dramatic (Fig. 2B, B'-B""). These differences were in line with our observation that *slc9a2* and *3* were expressed at lower levels during development, but they contrasted with the strong *slc9a2* and 3MO-induced fluid flow phenotype.

MCC-driven fluid flow depends on motile cilia formation as well as correct cilia directional beating imposed by basal bodies. In MCCs, basal bodies nucleate cilia, align the beating direction of cilia, and are also involved in F-actin formation and organization [Marshall, 2008; Wallingford, 2010; Antoniades et al., 2014], All these features are prerequisites to establish a forceful directional extracellular fluid flow. Therefore, we assessed basal body alignment and F-actin formation in *slc9a1, slc9a2* and *slc9a3* knockdowns. Injection of *centrin4-cfp* and *clamp-rfp* in combination with fluorescent labeling of F-actin was used to investigate basal bodies and actin in control and morphant embryos. In control-injected embryos, MCC basal bodies were uniformly aligned and apical F-actin was dense, but *slc9a1, 2* and *3* morphant MCCs displayed strongly reduced apical F-actin staining as well as randomized orientation of basal bodies (Fig. 2C). Basal body defects were most pronounced in *slc9a1*MO injected MCCs, in which they clustered in the center of the cell, while basal bodies in *slc9a2*MO or *slc9a3*MO injected cells tended to be more evenly spaced, but nevertheless lacked uniform alignment (Fig. 2C).

Previous reports linked cilia formation, apical actin organization and uniform basal body alignment in MCCs to Wnt/PCP signaling [Vladar et al., 2009; Wallingford, 2010], Furthermore, NHEs and other proton pumps were previously implicated in Wnt/PCP signaling [Simons et al., 2009; Niehrs, and Boutros, 2010], We next analyzed the impact of *slc9a* knockdown on neural tube closure in embryos, a classic assay to test for effects on Wnt/PCP-dependent convergent extension. Knockdown of *slc9a1, 2* or *3* individually and in combination revealed a high incidence of neural tube closure defects in manipulated embryos, as compared to either control injected embryos or the non-injected control side of individual embryos (Fig. 3A and S2A). In this assay, *slc9a1* and *2* knockdown were more efficient than *slc9a3* loss-of-function (Fig. 3A and S2A). Furthermore, combined knockdown caused a more severe phenotype than knockdown of each *slc9a* alone (Fig. 3A and S2A), suggesting synergistic yet not identical contributions of NHE1-3 to Wnt/PCP regulation. These data also provided the explanation for the strong effects of NHE loss-of-function on extracellular fluid flow generation.

In MCCs, Wnt/PCP is most prominently required for subapical actin-mediated linking of basal bodies, a prerequisite for uniform alignment in response to polarity signaling [Wallingford, 2010], In line with those accounts and our neural tube closure assay, analysis after individual or combined knockdown of *slc9a1-3* confirmed that in addition to ciliation and apical actin defects, NHE loss caused a lack of subapical actin links between basal bodies in MCCs (Fig. 3B). Lateral projections of confocal z-stacks further revealed strong effects on apical basal body transport in *slc9a1* and *2* morphant MCCs, mild effects after combined knockdown of *slc9a1-3*, and no defects in apical basal body positioning after *slc9a3* knockdown (Fig. 3B). While apical basal body transport is at least in part dependent on polarity signaling, the discrepancy between the strong effects of combined *slc9a1-3* knockdown on PCP-dependent neural tube closure and the relatively mild effects on apical basal body docking in the same sets of embryos suggested that additional non-PCP-related functions could be responsible for the severe basal body docking defects in *slc9a1* and 2 morphants.

Our previous data on the gastric H^+/K^+ATPase and the expression patterns of *slc9a* genes during epidermal development implied that NHEs could contribute to regulation of mucociliary gene expression in MCCs via the canonical Wnt/β-cat. signaling pathway as well. Therefore, we investigated if loss of NHE1, 2 or 3 function also affected the expression of the Wnt/β-cat. co-regulated ciliary transcription factor *foxj1*, which is required for motile cilia formation and basal body docking in MCCs [Gomperts et al., 2004; Stubbs et al., 2008; Walentek et al., 2012; Caron et al., 2012], Embryos were unilaterally injected with *slc9a1, 2 or 3* MOs and we analyzed gene expression by *in situ* hybridization. Expression levels were scored as decreased, unchanged or increased on the injected side as compared to the uninjected control side (Fig. 4A, B). knockdown of either *slc9a1* or *2* resulted in significant decrease in *foxj1* expression exclusively on the injected side, while *slc9a3* knockdown lead to increased *foxj1* expression (Fig. 4A, B). Loss of *foxj1* expression in *slc9a1* and 2 morphants could be either caused by reduced Wnt/β-cat. activity in differentiating MCCs or by reduced specification of MCCs by upstream transcription factors [Walentek, and Quigley, 2017], To reveal which of these two possibilities was responsible for the loss of *foxj1* expression, we analyzed expression of *foxi1e* in the epidermis, which is required for

specification of ion secreting cells, but whose expression is not dependent on the gastric H^+/K^+ATPase or canonical Wnt signaling [Walentek et al., 2015a], Neither loss of NHE1, 2 or 3 consistently caused reduction in *foxi1e* expression similar to *foxj1* (Fig. 4A, B), confirming that ion secreting cell specification did not rely on those proton pumps. Next, we quantified the numbers of MCCs and ion secreting cells in the epidermis according to cell type-characteristic morphological features after *slc9a* knockdown. This analysis revealed no changes in the proportions between MCCs and ion secreting cells in manipulated cells (Fig. S3A, B), strongly suggesting that reduced *foxj1* expression upon *slc9a1* and *2* knockdown was not a result of loss of MCC specification, but rather reflected decreased *foxj1* expression levels in differentiating MCCs. Collectively, these data implicated that NHE1 and 2 were required for efficient signaling through both Wnt/PCP as well as Wnt/β-cat. signaling branches causing ciliation and basal body defects by interfering with *foxj1*-dependent basal body docking as well as polarity-dependent actin organization and alignment of basal bodies. In contrast, NHE3 was dispensable for Wnt/β-cat.-dependent *foxj1* expression and basal body apical transport, but nevertheless required for Wnt/PCP-dependent actin regulation and basal body alignment.

Additionally, we investigated NHE loss-of-function effects on secretory cells by assessing *foxa1* expression, which is required for specification of small secretory cells [Quigley et al., 2011; Walentek et al., 2014; Dubaissi et al., 2014], and *otogelin* expression, which encodes a mucin-like compound produced by differentiated goblet cells [Hayes et al., 2007; Dubaissi et al., 2018], These experiments showed that knockdown of *slc9a1, 2* or *3* caused a loss of *foxa1* and small secretory cells, while *otogelin* expression was only markedly reduced in *slc9a2* morphants (Fig. 4A, B). Thus, our data further suggested that NHE1, 2 and 3 were all primarily required for normal MCC differentiation, with additional impact on mucociliary secretion, which could be either primary caused by dysregulated Wnt signaling or secondary to the loss of functional cilia.

Our data from NHE manipulations in the *Xenopus* model as well as published clinical data supported a function of NHEs in human airway mucociliary epithelia. Therefore, we next used air-liquid interface (ALI) culture of primary human airway epithelial cells (HAECs) to test the effects of pharmacological NHE inhibition on the regeneration of human respiratory epithelial cells [Gruenert et al., 1995; Fulcher et al., 2005], For that, we inhibited proton/sodium transport of NHE1, 2, 3 and 5 using the small molecule 5-(N-ethyl-N-isopropyl)-Amiloride (EIPA), which was added to the growth medium for a period of seven days during different phases of regeneration. Application of 25μM EIPA during early regeneration (ALI culture week 1) resulted in extensive cell death while vehicle treated controls developed normally (not shown). This was in line with previous reports of NHE inhibition leading to cell death [Fuster, and Alexander, 2014], as well as with our *Xenopus* data, which revealed extruded dead neural tube cells after knockdown of the strongly expressed *slc9a1* or after combined knockdown of *slc9a1, 2* and *3* (Fig. S2B). EIPA treatment during later stages of regeneration (ALI culture weeks 2-4) allowed us to analyze MCC ciliation and presence of basal stem cells by immunofluorescence as well as epithelial morphology by hematoxylin and eosin (H&E) staining. After EIPA treatment, cells were cultured without drug (week 2 and 3 treatments) until ALI day 28, when MCC ciliation is fully established. In vehicle treated controls, the apical surface of the epithelium was abundantly ciliated, but after EIPA

treatment in week 4, ciliation was strongly reduced (Fig. 5A, B). The effects of EIPA treatment were further confirmed in the *Xenopus* mucociliary epidermis, in which ciliogenesis, actin organization and mucus production were negatively affected exclusively in EIPA-treated specimens (Fig. S2C). It should be noted though, that drug treatments were less efficient and consistent than knockdown of *slc9a* transcripts in *Xenopus*, possibly reflecting reduced or more heterogeneous drug penetration from the apical side of the epithelium. EIPA treatment of HAECs during week 2 or 3 of regeneration also resulted in impaired regeneration and reduced MCC cilia formation (Fig. 5B, C). In contrast to ciliation defects, epithelialization in EIPA treated specimens appeared intact and Keratin 5-positive basal cells were detectable in all samples (Fig. 5B, C). Nevertheless, we observed a thinning of the epithelium in specimens treated during week 4 of regeneration, indicating impaired maintenance of epithelial cells immediately during/after drug application (Fig. 5B, C). These results strongly suggested an evolutionarily conserved role for NHEs in mucociliary development and regeneration. In particular, differentiation of MCCs relied on NHE function in both vertebrate mucociliary epithelia. Importantly, our data indicated that even transient NHE inhibition (week 2 or 3) affected differentiation ability during subsequent regeneration, and that MCC cilia were also affected when drug application started after initial formation of MCCs (week 4 treatment). Collectively, our experiments revealed a role for NHEs in cilia formation of MCCs, HAEC regeneration and the generation of extracellular fluid flow, which drives mucociliary clearance in various vertebrate epithelia, including the mammalian respiratory tract.

Discussion:

NHEs in Xenopus development

Here, we show that NHE1, 2 and 3 are required for normal mucociliary development in the *Xenopus* embryonic epidermis. All investigated NHEs seem to contribute to cellular pH homeostasis, which is necessary for overall development, signaling and gene expression. Loss of either NHE function by targeting each *slc9a* mRNA using MOs results in developmental phenotypes and breakdown of mucociliary clearance in tadpoles, which could be primarily attributed to defective differentiation of MCCs. While we did not perform rescue experiments, the specificity of treatments is supported by differential effects induced by the different *slc9a* MOs, which are likely due to different levels and the timing of expression of the different *slc9a* transcripts. Most prominently, mucociliary gene expression is altered, but in some cases, knockdown causes a decrease in expression while in other cases it leads to increased expression of *foxj1*. Furthermore, combined low-level knockdown of all three *slc9a* transcripts resulted in a more dramatic phenotype in later development, but a milder MCC cilia phenotype strongly suggesting synergy of NHEs (and their loss-of-function effects) depending on expression levels within the targeted tissues. Together, these data argue for specific and differential contributions of NHEs to cellular homeostasis and potentially signaling regulation.

NHEs and mucociliary Wnt signaling

Multiple proton transporters, including NHEs, are implicated in Wnt signaling regulation. In *Xenopus* and human cells, the vacuolar H^+ATPase was suggested to regulate canonical and

non-canonical Wnt signaling activation through acidification of Wnt signalosomes, i.e. early endosomes that are taken up by the cell upon ligand binding to signaling receptors [Cruciat et al., 2010], Furthermore, *Drosophila melanogaster* NHE2 as well as human NHE3 were shown to be required for recruitment of the intracellular Wnt pathway component Dishevelled to the membrane, which is necessary for downstream Wnt signaling processes, including signalosome formation, Wnt/β-cat. and Wnt/PCP signaling [Simons et al., 2009; Niehrs, and Boutros, 2010], The gastric H^+/K^+ATPase is also required for Wnt/β-catenin and Wnt/PCP signaling dependent processes in *Xenopus* embryos, including *foxj1* expression, basal body alignment and generation of extracellular fluid flow [Walentek et al., 2012; Walentek et al., 2015a], Therefore, our data on NHEs support the hypothesis that NHEs also contribute to Wnt signaling regulation in the *Xenopus* mucociliary epidermis.

Impaired Wnt signaling activation upon loss of NHE function could also provide an explanation as to why we observe overlapping but not identical effects at the level of cell type gene expression and MCC differentiation: loss of NHE1 and 2 likely affect canonical Wnt/β-cat. signaling and Wnt/PCP signaling leading to reduced *foxj1* expression and defective alignment of basal bodies, respectively. In contrast, loss of NHE3 seemed to affect only Wnt/PCP-dependent alignment of basal bodies. This could be attributed to differences in expression dynamics between the different *slc9a* family members and the enhanced sensitivity of polarity signaling to manipulations. *slc9a1* is expressed most strongly (maternally and specifically in the epidermis) and its knockdown consistently induced the most severe phenotypes. *slc9a2* is expressed at lower levels but shows significant expression in the epidermis from early neurula stages onwards. *slc9a3* is expressed at the lowest level in the epidermis and maternally deposited transcripts likely represent the population of mRNAs mainly affecting epidermal cells, because zygotic expression is predominantly restricted to the endoderm during MCC differentiation stages.

NHE function in human airway cells

Importantly, our HAEC data also shows that transient inhibition of NHEs as well as their inhibition after initial MCC differentiation can lead to impaired ciliation and, consequently, airway clearance insufficiency. Impaired MCC cilia formation could explain why *SLC9A3* mutations were identified as additional risk factors in cystic fibrosis patients. Multiple studies have detected an increase in morbidity in cystic fibrosis patients with additional mutations in *SLC9A3*, including a higher risk for airway infections in children and adults [Pereira et al., 2017b; Dorfman et al., 2011; Corvol et al., 2015; Li et al., 2014]. These findings suggest that NHE3 might also regulate Wnt signaling and gene expression in the respiratory epithelium, and it will be interesting to further explore that possibility in future studies. It will be also important to further investigate the precise effects of *slc9a1-3* knockdown and NHE manipulation on Wnt signaling activation, including the level and timing of signaling alterations in human and *Xenopus* mucociliary cells.

Taken together, our work contributes novel important insights into the role of NHEs in vertebrate development and disease, links NHE function to motile cilia formation in MCCs, and suggests a role for NHEs in Wnt signaling modulation in mucociliary epithelia.

Supplementary Material

Refer to Web version on PubMed Central for supplementary material.

Acknowledgements:

We thank E. Pangilinan, L. Zlock and S. Schefold for expert technical support during the study. We also thank the Light Imaging Center at the University of Freiburg for microscope use as well as P. Lishko for using GX-1 Memrecam. We especially thank Terry Machen for his support and discussions. DIS was supported by the URAP program at UC Berkeley and a Pergo Foundation SURF L&S fellowship. GB was supported through the Amgen Scholars Program. MH and AT were supported through DFG grant WA 3365/2-1 to PW. Xenopus work in the Harland lab was funded through NIH grant GM042341. Work in the Finkbeiner lab was supported through NIH grant DK072517 and Cystic Fibrosis Foundation grant VERKMA 15R0. PW was funded by a DFG postdoctoral fellowship (WA 3365/1-1), a Pathway to Independence Award by the NHLBI (K99HL127275), and work in the Walentek lab is funded through the Emmy Noether Program by the DFG WA 3365/2-1.

Bibliography:

Antoniades I, Stylianou P, Skourides PA: Making the Connection: Ciliary Adhesion Complexes Anchor Basal Bodies to the Actin Cytoskeleton. Dev Cell 2014;28:70–80. [PubMed: 24434137]

Brooks ER, Wallingford JB: Multiciliated Cells. Curr Biol 2014;24:R973–R982. [PubMed: 25291643]

Caron A, Xu X, Lin X: Wnt/β-catenin signaling directly regulates Foxj1 expression and ciliogenesis in zebrafish Kupffer's vesicle. Development 2012;139:514–24. [PubMed: 22190638]

Corvol H, Blackman SM, Boëlle PY, Gallins PJ, Pace RG, Stonebraker JR, et al.: Genome-wide association meta-analysis identifies five modifier loci of lung disease severity in cystic fibrosis. Nat Commun 2015;6:1–8.

Cruciat C-M, Ohkawara B, Acebron SP, Karaulanov E, Reinhard C, Ingelfinger D, et al.: Requirement of prorenin receptor and vacuolar H+-ATPase-mediated acidification for Wnt signaling. Science 2010;327:459–63. [PubMed: 20093472]

Dorfman R, Taylor C, Lin F, Sun L, Sandford A, Paré P, et al.: Modulatory effect of the SLC9A3 gene on susceptibility to infections and pulmonary function in children with cystic fibrosis. Pediatr Pulmonol 2011;46:385–92. [PubMed: 20967843]

Dubaissi E, Rousseau K, Hughes GW, Ridley C, Grencis RK, Roberts IS, et al.: Functional characterization of the mucus barrier on the *Xenopus tropicalis* skin surface. Proc Natl Acad Sci 2018;115:726–731. [PubMed: 29311327]

Dubaissi E, Rousseau K, Lea R, Soto X, Nardeosingh S, Schweickert A, et al.: A secretory cell type develops alongside multiciliated cells, ionocytes and goblet cells, and provides a protective, anti-infective function in the frog embryonic mucociliary epidermis. Development 2014;141:1514–25. [PubMed: 24598166]

Fulcher ML, Gabriel S, Burns K, Yankaskas JR, Randell SH: Well-differentiated human airway epithelial cell cultures. Methods Mol Med 2005;107:183–206. [PubMed: 15492373]

Fuster DG, Alexander RT: Traditional and emerging roles for the SLC9 Na+/H+ exchangers. Pflügers Arch - Eur J Physiol 2014;466:61–76. [PubMed: 24337822]

Gomperts BN, Gong-Cooper X, Hackett BP: Foxj1 regulates basal body anchoring to the cytoskeleton of ciliated pulmonary epithelial cells. J Cell Sci 2004;117:1329–37. [PubMed: 14996907]

Gruenert DC, Finkbeiner WE, Widdicombe JH: Culture and transformation of human airway epithelial cells. Am J Physiol 1995;268:L347–60. [PubMed: 7900815]

Harguindey S, Orive G, Luis Pedraz J, Paradiso A, Reshkin SJ: The role of pH dynamics and the Na +/H+ antiporter in the etiopathogenesis and treatment of cancer. Two faces of the same coin--one single nature. Biochim Biophys Acta 2005;1756:1–24. [PubMed: 16099110]

Harland RM: In situ hybridization: an improved whole-mount method for Xenopus embryos. Methods Cell Biol 1991;36:685–95. [PubMed: 1811161]

Hayes JM, Kyoung S, Abitua PB, Joo T, Herrington ER, Kitayama A, et al.: Identification of novel ciliogenesis factors using a new in vivo model for mucociliary epithelial development 2007;312:115–130.

Li W, Soave D, Miller MR, Keenan K, Lin F, Gong J, et al.: Unraveling the complex genetic model for cystic fibrosis: pleiotropic effects of modifier genes on early cystic fibrosis-related morbidities. Hum Genet 2014;133:151–61. [PubMed: 24057835]

Ma L, Quigley I, Omran H, Kintner C: Multicilin drives centriole biogenesis via E2f proteins. Genes Dev 2014;28:1461–1471. [PubMed: 24934224]

Marshall WF: Basal Bodies : Platforms for Building Cilia. Curr Top Dev Biol 2008;85:1–22. [PubMed: 19147000]

Mitchell B, Stubbs JL, Huisman F, Taborek P, Yu C, Kintner C: The PCP Pathway Instructs the Planar Orientation of Ciliated Cells in the Xenopus Larval Skin. Curr Biol 2009;19:924–929. [PubMed: 19427216]

Namkung W, Finkbeiner WE, Verkman AS: CFTR-Adenylyl Cyclase I Association Responsible for UTP Activation of CFTR in Well-Differentiated Primary Human Bronchial Cell Cultures. Mol Biol Cell 2010;21:2639–2648. [PubMed: 20554763]

Niehrs C, Boutros M: Trafficking, acidification, and growth factor signaling. Sci Signal 2010;3:pe26. [PubMed: 20699474]

Ozkucur N, Song B, Bola S, Zhang L, Reid B, Fu G, et al.: NHE3 phosphorylation via PKCη marks the polarity and orientation of directionally migrating cells. Cell Mol Life Sci 2014;71:4653–63. [PubMed: 24788043]

Park TJ, Mitchell BJ, Abitua PB, Kintner C, Wallingford JB: Dishevelled controls apical docking and planar polarization of basal bodies in ciliated epithelial cells. Nat Genet 2008;40:871–879. [PubMed: 18552847]

Pereira SVN, Ribeiro JD, Bertuzzo CS, Marson FAL: Association of clinical severity of cystic fibrosis with variants in the SLC gene family (SLC6A14, SLC26A9, SLC11A1 and SLC9A3). Gene 2017a;629:117–126. [PubMed: 28756021]

Quigley IK, Kintner C: Rfx2 stabilizes Foxj1 binding at chromatin loops to enable multiciliated cell gene expression. Plos Genetic 2016 DOI: 10.1101/085571

Quigley IK, Stubbs JL, Kintner C: Specification of ion transport cells in the Xenopus larval skin. Development 2011;714:705–714.

Schneider L, Stock C, Dieterich P, Jensen BH, Pedersen LB, Satir P, et al.: The Na+/H+ exchanger NHE1 is required for directional migration stimulated via PDGFR-a in the primary cilium. J Cell Biol 2009;185:163–176. [PubMed: 19349585]

Schreiber R: Ca2+ signaling, intracellular pH and cell volume in cell proliferation. J Membr Biol 2005;205:129–37. [PubMed: 16362501]

Sera A, Moroni N, Psaila R, Zonfrillo M, Andreola F, Wannenes F, et al.: Anti-proliferative effect of atrial natriuretic peptide on colorectal cancer cells: evidence for an Akt-mediated cross-talk between NHE-1 activity and Wnt/β-catenin signaling. Biochim Biophys Acta 2012;1822:1004–18. [PubMed: 22387884]

Session AM, Uno Y, Kwon T, Chapman JA, Toyoda A, Takahashi S, et al.: Genome evolution in the allotetraploid frog Xenopus laevis. Nature 2016;538:336–343. [PubMed: 27762356]

Simons M, Gault WJ, Gotthardt D, Rohatgi R, Klein TJ, Shao Y, et al.: Electrochemical cues regulate assembly of the Frizzled/Dishevelled complex at the plasma membrane during planar epithelial polarization. Nat Cell Biol 2009;11:286–94. [PubMed: 19234454]

Sive HL, Grainger RM, Harland RM: Early Development of Xenopus laevis, Cold Spring Harbor, NY, USA, Cold Spring Harbor Laboratory Press, 2000 DOI: 10.1101/pdb.prot5536

Siyanov V, Baltz JM: NHE1 is the sodium-hydrogen exchanger active in acute intracellular pH regulation in preimplantation mouse embryos. Biol Reprod 2013;88:157. [PubMed: 23677982]

Slepkov ER, Rainey JK, Sykes BD, Fliegel L: Structural and functional analysis of the Na+/H+ exchanger. Biochem J 2007;401:623–33. [PubMed: 17209804]

Souza SD, Garcia-Cabado A, Yu F, Teter K, Lukacs G, Skorecki K, et al.: The epithelial sodium-hydrogen antiporter Na+/H+ exchanger 3 accumulates and is functional in recycling endosomes. J Biol Chem 1998;273:2035–43. [PubMed: 9442041]

Stubbs JL, Oishi I, Izpisúa Belmonte JC, Kintner C, Stubbs JL, Oishi I, et al.: The forkhead protein Foxj1 specifies node-like cilia in Xenopus and zebrafish embryos. Nat Genet 2008;40:1454–60. [PubMed: 19011629]

Stubbs JL, Vladar EK, Axelrod JD, Kintner C: Multicilin promotes centriole assembly and ciliogenesis during multiciliate cell differentiation. Nat Cell Biol 2012;14:1–10.

Vladar EK, Antic D, Axelrod JD: Planar cell polarity signaling: the developing cell's compass. Cold Spring Harb Perspect Biol 2009;1:a002964. [PubMed: 20066108]

Walentek P, Beyer T, Hagenlocher C, Müller C, Feistel K, Schweickert A, et al.: ATP4a is required for development and function of the Xenopus mucociliary epidermis - a potential model to study proton pump inhibitor-associated pneumonia. Dev Biol 2015a;408:292–304. [PubMed: 25848696]

Walentek P, Beyer T, Thumberger T, Schweickert A, Blum M: ATP4a is required for Wnt-dependent Foxj1 expression and leftward flow in Xenopus left-right development. Cell Rep 2012;1:516–27. [PubMed: 22832275]

Walentek P, Bogusch S, Thumberger T, Vick P, Dubaissi E, Beyer T, et al.: A novel serotonin-insecreting cell type regulates ciliary motility in the mucociliary epidermis of Xenopus tadpoles. Development 2014;141:1526–1533. [PubMed: 24598162]

Walentek P, Boutin C, Kodjabachian L: Planar Cell Polarity in Ciliated Epithelia; in : Cell Polarity in Development and Disease. 2017, pp 177–209.

Walentek P, Hagenlocher C, Beyer T, Müller C, Feistel K, Schweickert A, et al.: ATP4 and ciliation in the neuroectoderm and endoderm of Xenopus embryos and tadpoles. Data Br 2015b;4:22–31.

Walentek P, Quigley IK: What we can learn from a tadpole about ciliopathies and airway diseases: Using systems biology in Xenopus to study cilia and mucociliary epithelia. Genesis 2017;55 DOI: 10.1002/dvg.23001

Walentek P, Quigley IK, Sun DI, Sajjan UK, Kintner C, Harland RM: Ciliary transcription factors and miRNAs precisely regulate Cp110 levels required for ciliary adhesions and ciliogenesis. Elife 2016;5:1–24.

Wallingford JB: Planar cell polarity signaling, cilia and polarized ciliary beating. Curr Opin Cell Biol 2010;22:597–604. [PubMed: 20817501]

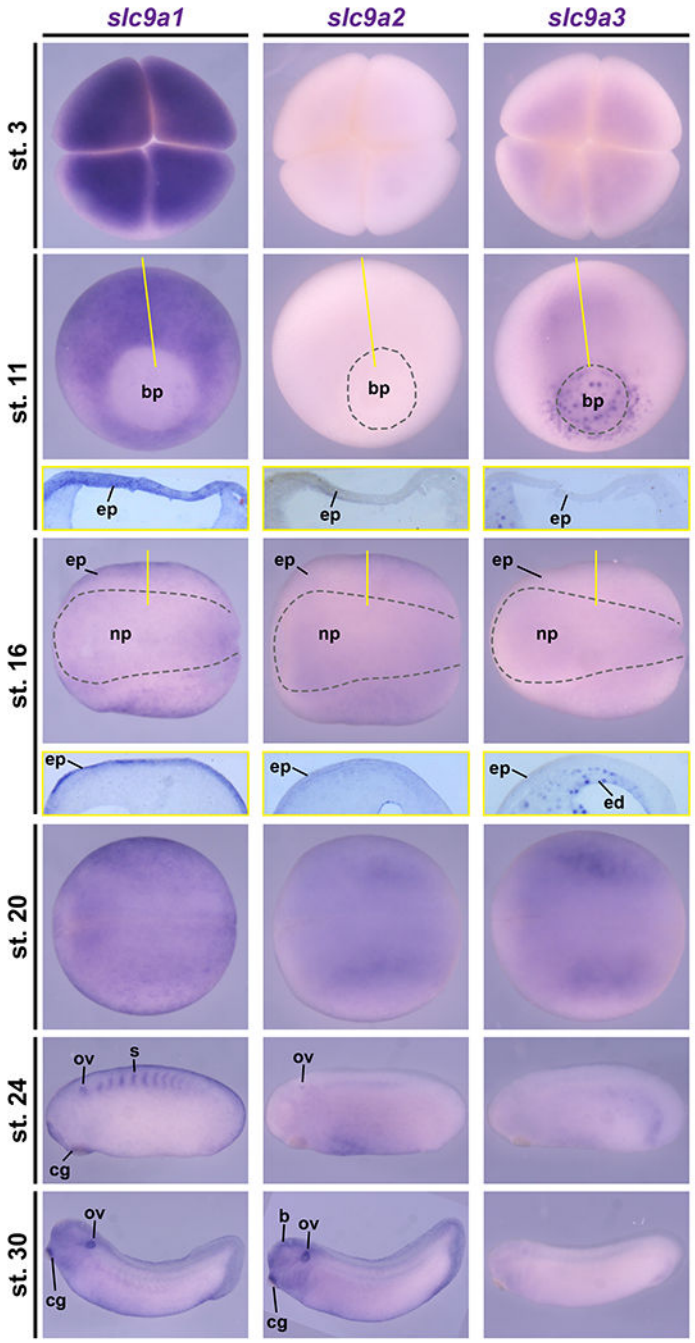

Figure 1: Dynamic *slc9a1, 2* and *3* expression during *Xenopus* development

In situ hybridization on *Xenopus laevis* embryos from stages (st.) 3 – 30 revealed dynamic expression of *slc9a* transcripts during early development. At the four-cell stage (st. 3) strong maternal transcript deposition was detected for *slc9a1*, but *slc9a3* was only lowly expressed and no signals were observed for *slc9a2.* During gastrulation (st. 11), *slc9a1* was markedly expressed throughout the prospective ectoderm and mesoderm, while *slc9a3* was found at the blastpore (bp), the endoderm as well as involuting mesodermal cells and no specific expression was found for *slc9a2.* In neurula stage embryos (st. 16 and 20), *slc9a1* and 2

transcripts were detected in the epidermal ectoderm (ep) with stronger expression of *slc9a1*, and *slc9a3* was expressed in the endoderm (ed). During late neurulation (st. 20), *slc9a2* and *3* were also expressed in the presomitic mesoderm. In tailbud stages (st. 24, 30), *slc9a1* and 2 transcripts were detected in the otic vesicle (ov) and the cement gland (eg), but not *slc9a3.* Additionally, *slc9a1* was expressed in the somites (s), and *slc9a2* was expressed in the brain (b). St. 3 embryos are depicted in animal view. St. 11 embryos are depicted in vegetal view, dorsal up. St. 16 and 20 embryos are depicted in dorsal view, anterior left. St. 24 and 30 embryos are depicted in lateral view, anterior left. Sections depicting the epidermis of st. 11 and st. 16 embryos are shown in yellow boxes below the whole mount image. Section planes are indicated by yellow lines.

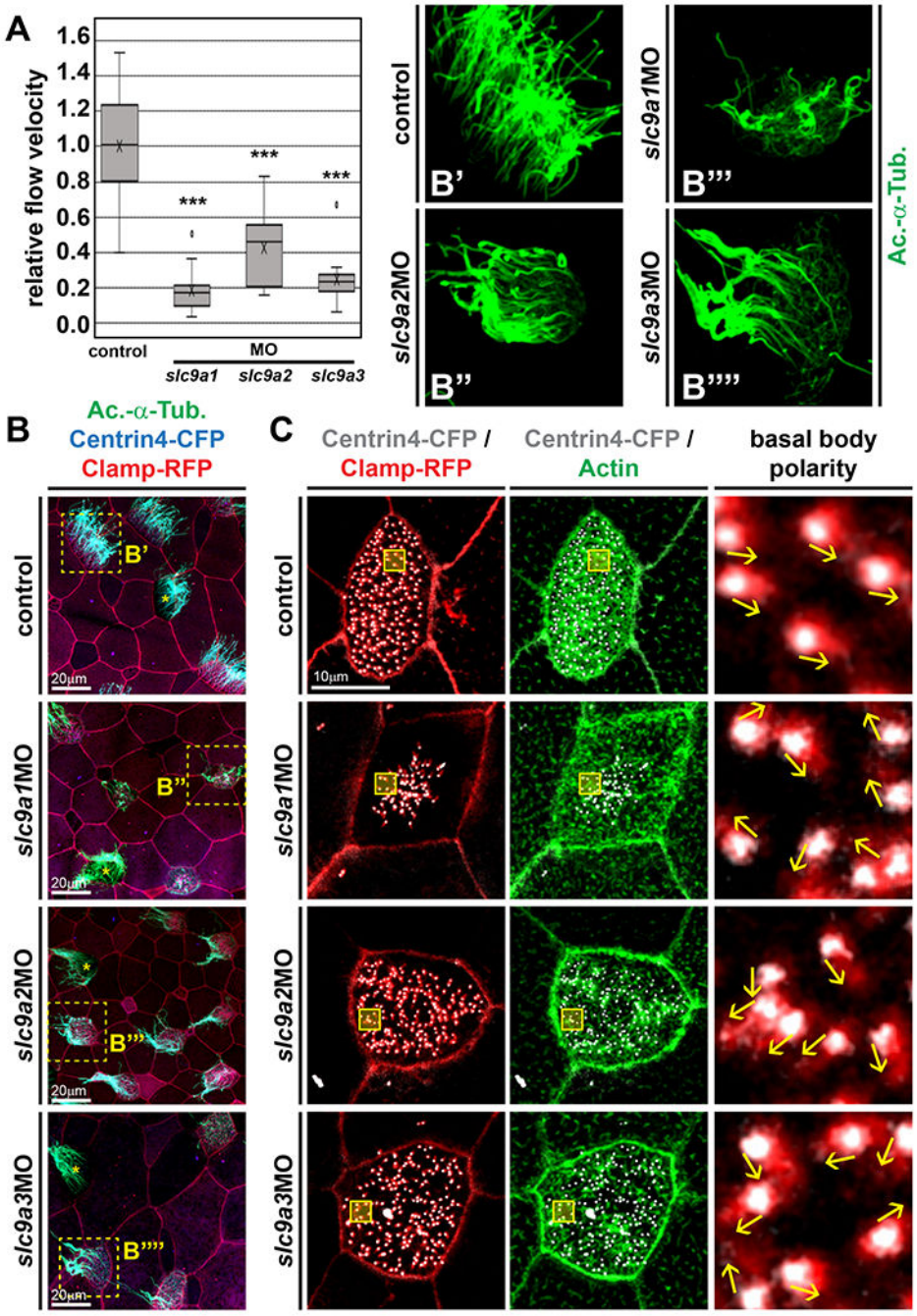

Figure 2: NHE1-3 Ioss-of-function impairs fluid flow, MCC cilia formation and basal body alignment

(**A**) Extracellular fluid flow was quantified by addition of fluorescent beads to the medium and high-speed fluorescent microscopy for at least 10s at 50 – 100 frames per second. Uninjected embryos were used as controls (n = 15). Morphants were injected with the indicated MO (6 pmol). *slc9a1*MO, n = 13; *slc9a2*MO, n = 16; *slc9a3*MO, n = 14. Flow velocities were calculated relative to median values of uninjected controls. Boxes depict 50% of values, the median is depicted by the horizontal line, the mean is depicted by the

cross. Whiskers indicate the upper and lower quartiles, outliers are depicted as circles. *** = *P<0.001*, Mann-Whitney test. (**B**) Embryos were injected with *centrin4-cfp* (blue) and *clamp-rfp* (red) mRNAs (control) to visualize cell borders and to identify targeted cells. Morphants were co-injected with 6 pmol of the indicted MO. Cilia were visualized by immunofluorescence staining against acetylated-α-tubulin (Ac.-α-Tub., green). Dashed boxes in micrographs on the left indicate magnified areas shown in B'-B'". Non-targeted MCCs are indicated by asterisks. (**C**) Embryos were injected with *centrin4-cfp* (grey) and *clamp-rfp* (red) mRNAs (control) to visualize basal bodies and rootlets, respectively. Morphants were co-injected with 6 pmol of the indicted MO. F-actin was visualized by fluorescence staining with phalloidin (green). Boxes in micrographs on the left indicate magnified areas shown in the right panels. Direction of basal bodies is indicated by arrows. Scale bars indicate magnification.

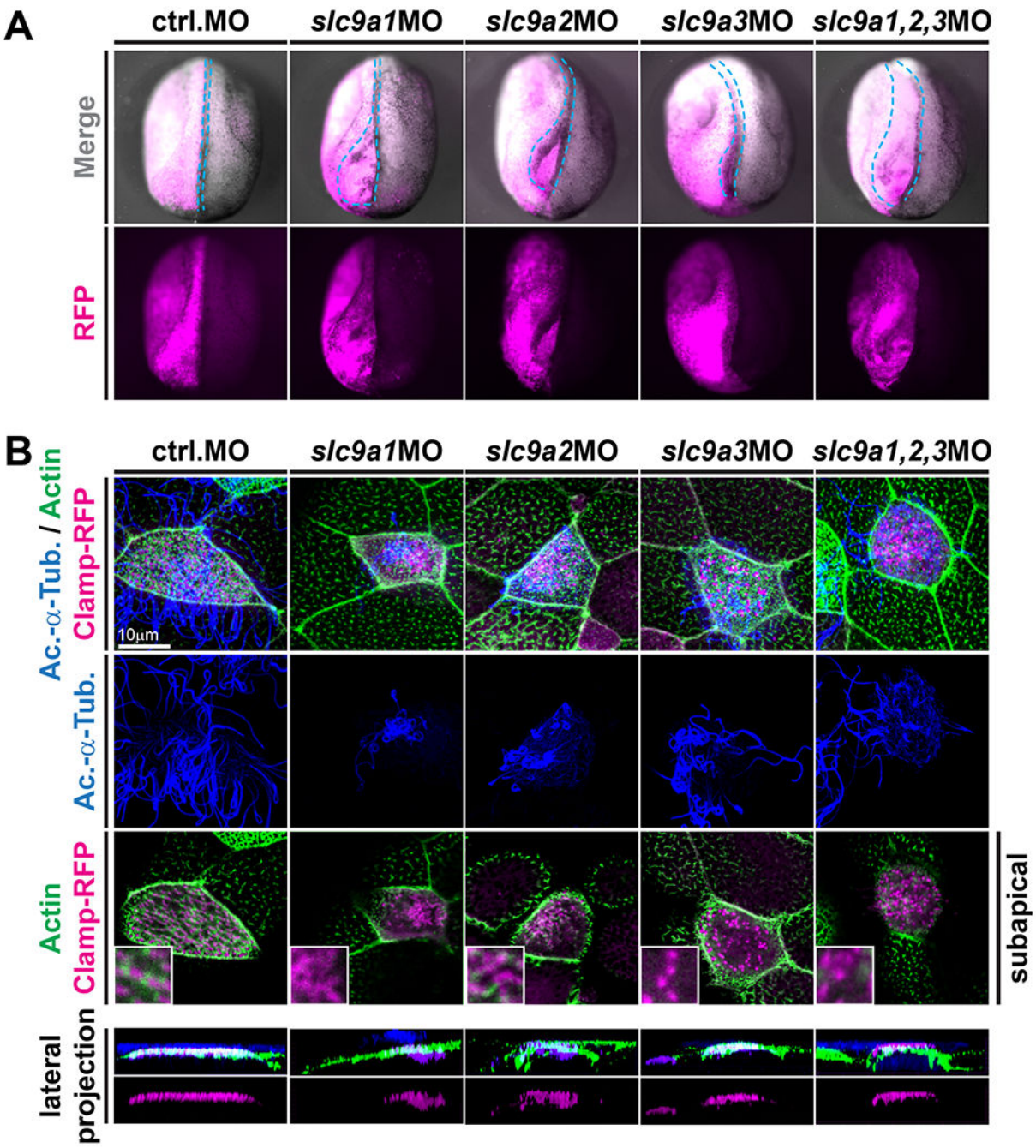

Figure 3: NHE1-3 loss-of-function affects neural tube closure as well as subapical actin formation and basal body positioning in MCCs

(**A**) *slc9a1. 2* or *3* were knocked down unilaterally (visualized by co-injection of RFP encoding mRNA; individual knockdown at 4pmol, combined knockdown at 1.33pmol of each MO) and neural tube closure was analyzed at stage 19-20. In contrast to control-injected embryos and the non-injected control side of individual embryos, *slc9a* morphants displayed various degrees of neural tube closure defects (quantified in Fig. S2A). Representative examples are shown in anterior-dorsal view and the outline of the injected

neural folds is marked by dashed blue line. (**B**) Embryos were injected with *clamp-rfp* (red) mRNAs and indicated MOs (same set of embryos as depiced in A). Immunofluorescence staining against acetylated-α-tubulin (Ac.-α-Tub., blue) revealed cilia and phalloidin stained the actin cytoskeleton (green). Loss of NHE function induced cilia defects as well as loss of subapical actin links between basal bodies in all treatments. Lateral projections further revealed severe basal body apical transport defects in *slc9a1* and *2* morphants, but only mild or no defects after combined knockdown or after *slc9a3*MO injections. Scale bars indicate magnification.

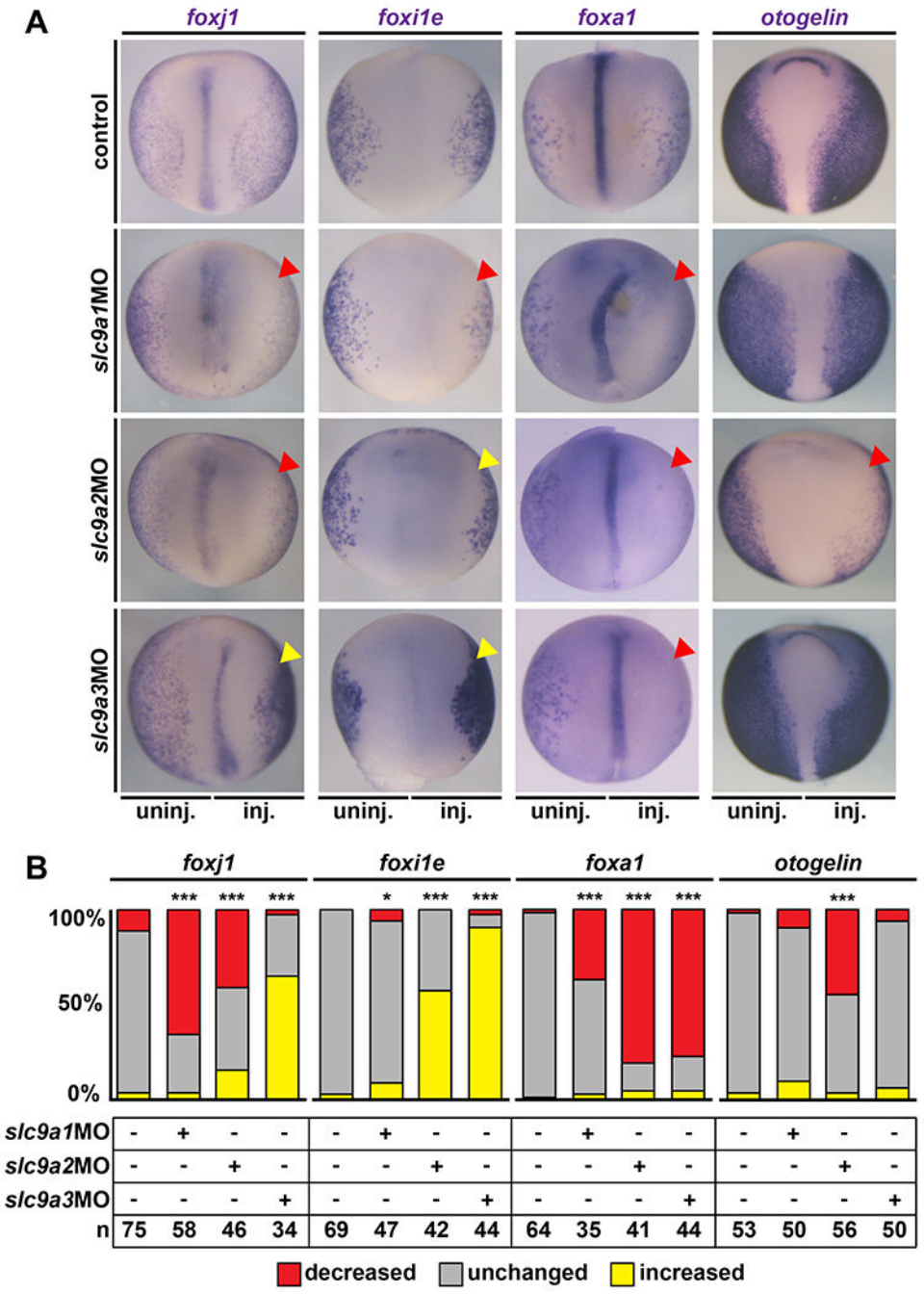

Figure 4: NHE1-3 Ioss-of-function affects gene expression in MCCs and secretory cells of the mucociliary epidermis

In situ hybridization for cell type markers in the embryonic mucociliary epidermis. Embryos were injected unilaterally on the right side (inj.) and the uninjected left side (uninj.) served as internal control. Unmanipulated specimens were used as additional controls (control). (**A**) St. 17 embryos are shown in dorsal view, anterior up. *foxj1* marks MCCs, *foxi1e* marks ion secreting cells, *foxa1* marks small secretory cells and *otogelin* is a marker of mucus secreting goblet cells. Downregulation is indicated by red arrowheads, upregulation is

indicated by yellow arrowheads. (**B**) Quantification of results. * = *P<0.05*, *** = *P<0.001*, chi-squared test.

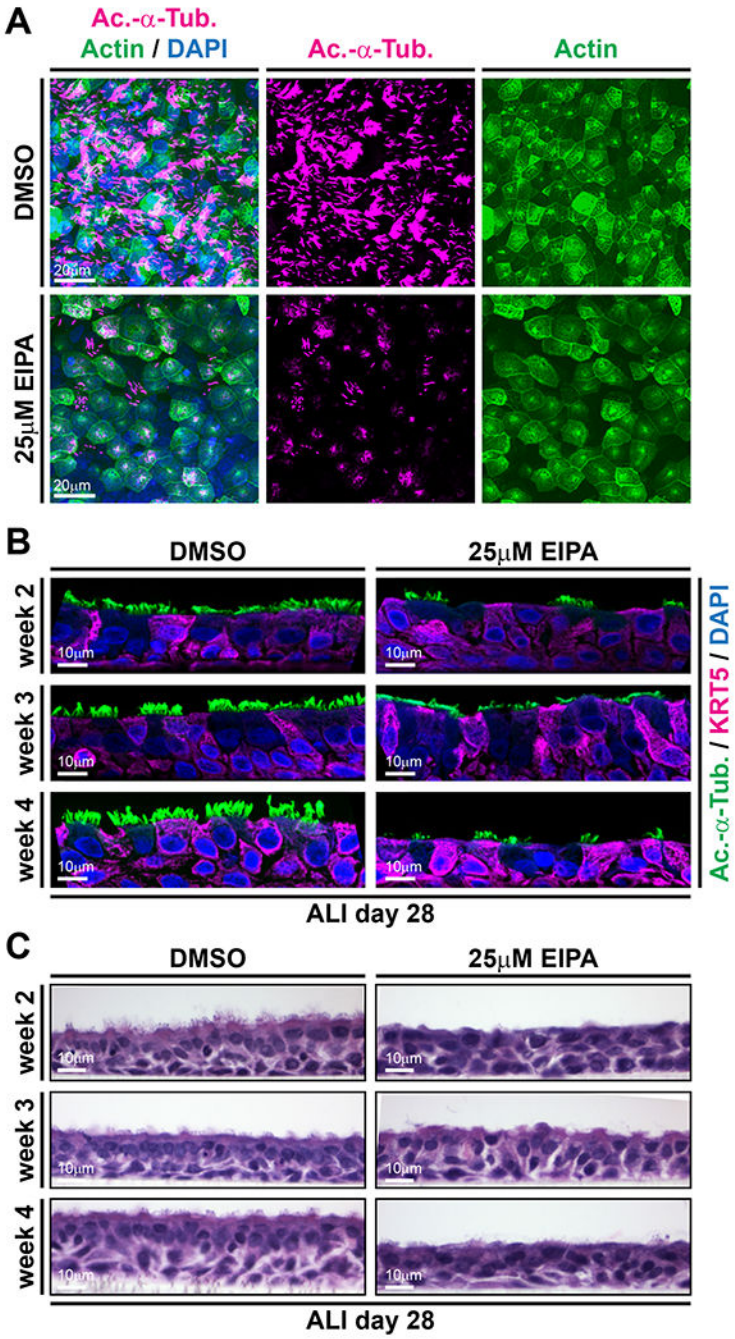

Figure 5: Pharmacological inhibition of NHE function impairs MCC cilia formation and regeneration in human airway epithelial cells

Human airway epithelial cells (HAECs) were grown in ALI cultures and treated either with vehicle (DMSO controls) or 25μM of the NHE inhibitor El PA for seven days. (**A**) Top view on cultured cells at ALI day 28 after seven days of treatment during week 4 of regeneration. Immunofluorescence staining for MCC cilia (Ac.-α-Tub., magenta), F-actin (green) and nuclei (DAPI, blue) revealed defective MCC ciliation in EIPA-treated specimens. Scale bars indicate magnification. (**B**) Immunofluorescence staining for MCC cilia (Ac.-α-Tub., green), Keratin 5-positive basal cells (KRT5, magenta) and nuclei (DAPI, blue) revealed ciliation

defects in EIPA-treated specimens, but no loss of basal cells. Scale bars indicate magnification. Morphology of control (DMSO) and El PA treated HAECs at ALI day 28, after treatment during the indicated week of regeneration revealed successful epithelialization of HAECs in controls and EIPA-treated specimens. Fixation directly after El PA treatment (week 4) further revealed a thinning of the epithelium. Apical surface up. Scale bars indicate magnification.